

REPORT DOCUMENTATION PAGE

Form Approved
OMB No. 0704-0188

Public reporting burden for this collection of information is estimated to average 1 hour per response, including the time for reviewing instructions, searching existing data sources, gathering and maintaining the data needed, and completing and reviewing this collection of information. Send comments regarding this burden estimate or any other aspect of this collection of information, including suggestions for reducing this burden to Department of Defense, Washington Headquarters Services, Directorate for Information Operations and Reports (0704-0188), 1215 Jefferson Davis Highway, Suite 1204, Arlington, VA 22202-4302. Respondents should be aware that notwithstanding any other provision of law, no person shall be subject to any penalty for failing to comply with a collection of information if it does not display a currently valid OMB control number. **PLEASE DO NOT RETURN YOUR FORM TO THE ABOVE ADDRESS.**

1. REPORT DATE (DD-MM-YYYY) 05-08-2008		2. REPORT TYPE Technical Paper		3. DATES COVERED (From - To)	
4. TITLE AND SUBTITLE Constrained Trajectory Optimization Using Pseudospectral Methods (Preprint)				5a. CONTRACT NUMBER	
				5b. GRANT NUMBER	
				5c. PROGRAM ELEMENT NUMBER	
6. AUTHOR(S) Tim Jorris (USAF TPS/CS); Chris Schulz (AFRL/RZST); Franklin Friedl (Spiral/Jackson and Tull); Anil V. Rao (University of Florida)				5d. PROJECT NUMBER	
				5e. TASK NUMBER	
				5f. WORK UNIT NUMBER 48470255	
7. PERFORMING ORGANIZATION NAME(S) AND ADDRESS(ES) Air Force Research Laboratory (AFMC) AFRL/RZST 4 Draco Drive Edwards AFB CA 93524-7160				8. PERFORMING ORGANIZATION REPORT NUMBER AFRL-RZ-ED-TP-2008-327	
9. SPONSORING / MONITORING AGENCY NAME(S) AND ADDRESS(ES) Air Force Research Laboratory (AFMC) AFRL/RZS 5 Pollux Drive Edwards AFB CA 93524-7048				10. SPONSOR/MONITOR'S ACRONYM(S)	
				11. SPONSOR/MONITOR'S NUMBER(S) AFRL-RZ-ED-TP-2008-327	
12. DISTRIBUTION / AVAILABILITY STATEMENT Approved for public release; distribution unlimited (PA #08308A).					
13. SUPPLEMENTARY NOTES For presentation at the AIAA Guidance, Navigation, and Controls Conference, to be held in Honolulu, HI, 18-21 Aug 2008.					
14. ABSTRACT A constrained optimized trajectory is required to satisfy a hypersonic reentry vehicle's mission requirements and operating limitations. Specified initial and final conditions commonly define a two-point boundary value problem. Such problems have established solution techniques implemented in software packages developed by the National Aeronautics and Space Administration. Current research has demonstrated the use of pseudospectral methods to converge to constrained optimal reentry trajectories. Gauss Pseudospectral Optimal Control Software (GPOCS) ¹⁻³ is used for this research, however, DIDO is another valid software package implementing pseudospectral methods. The research herein documents the implementation of GPOCS and compares the results, and solution convergence, with those from the Program to Optimize Simulated Trajectories (POSTII). This paper also addresses the robust ability of GPOCS to incorporate multiple phases as well as phase-dependent constraints.					
15. SUBJECT TERMS					
16. SECURITY CLASSIFICATION OF:			17. LIMITATION OF ABSTRACT	18. NUMBER OF PAGES	19a. NAME OF RESPONSIBLE PERSON
a. REPORT	b. ABSTRACT	c. THIS PAGE			Mr. Roy Hilton
Unclassified	Unclassified	Unclassified	SAR	34	19b. TELEPHONE NUMBER (include area code) N/A

Constrained Trajectory Optimization Using Pseudospectral Methods

Timothy R. Jorris *

US Air Force Test Pilot School, 220 S Wolfe Ave, Edwards Air Force Base, CA 93524

Christopher S. Schulz † and Franklin R. Friedl ‡

Air Force Research Laboratory, 4 Draco Dr., Edwards Air Force Base, CA 93524

Anil V. Rao §

University of Florida, P.O. Box 116250, Gainesville, FL 32611

A constrained optimized trajectory is required to satisfy a hypersonic reentry vehicle's mission requirements and operating limitations. Specified initial and final conditions commonly define a two-point boundary value problem. Such problems have established solution techniques implemented in software packages developed by the National Aeronautics and Space Administration. Current research has demonstrated the use of pseudospectral methods to converge to constrained optimal reentry trajectories. Gauss Pseudospectral Optimal Control Software (GPOCS)¹⁻³ is used for this research, however, DIDO is another valid software package implementing pseudospectral methods. The research herein documents the implementation of GPOCS and compares the results, and solution convergence, with those from the Program to Optimize Simulated Trajectories (POST II). This paper also addresses the robust ability of GPOCS to incorporate multiple phases as well as phase-dependent constraints.

*Major, USAF, Member AIAA, timothy.jorris@us.af.mil

†Captain, USAF, Member AIAA

‡System Analyst, Spiral Technologies, Lancaster, CA, 93535, Member AIAA

§Assistant Professor, Department of Mechanical and Aerospace Engineering; anilvrao@ufl.edu, Member AIAA

The views expressed in this paper are those of the authors and do not reflect the official policy or position of the United States Air Force, the Department of Defense, or the U.S. Government.

This material is declared a work of the U.S. Government and is not subject to copyright protection in the United States. APPROVED FOR PUBLIC RELEASE, DISTRIBUTION UNLIMITED

I. Introduction

The optimal trajectory of a maneuvering hypersonic reentry vehicle, such as the Space Shuttle, is generated as the solution to a constrained two point boundary value problem. The boundary value problem is formulated via identifying both initial and final conditions, such as launch and landing geographic locations. Furthermore, the problem is constrained by limiting angle of attack, aerodynamic heating, and setting upper and lower boundaries on altitude. These conditions define the Hessian from which the optimal solution of the boundary value problem is solved.

While analytical methods exist to solve a range of elementary boundary value problems, the complexity of problems such as a hypersonic vehicle reentry trajectory are better suited to numerical methods. This approach is well established in dedicated trajectory generation codes such as NASA-Langley's Program to Optimize Simulated Trajectories (POST) and NASA-Glenn's Optimal Trajectories by Implicit Simulations (OTIS). While the approaches to solving the boundary value problem differ, both of the above mentioned codes have been shown by Nelson⁴ to produce nearly identical numerical results in the case of minimally constrained trajectories. In the case of a more heavily constrained problem, however, the solutions from the two codes may begin to diverge in solution, or have the case when one fails to converge on a solution altogether.

The necessity to increase the number of constraints on a reentry trajectory is reliant on the definition of the mission of the reentry vehicle. In the case of the Space Shuttle, the solution space is constrained by the physical constraints mentioned above, but with few if any intermediate waypoint constraints. In the case of a more demanding mission profile additional constraints are levied on the problem. These can include physical constraints such as maximizing the lift to drag ratio in order to maximize the down range capability of the vehicle. Additional constraints can also be geographic in nature, such as avoiding overflight of specified airspace. Due to these additional constraints the ability to converge to an optimal solution becomes dependent on the numeric method used.

The objective of this paper is to demonstrate the ability of pseudospectral method to converge to a constrained optimal reentry trajectory in ever increasing levels of constraint complexity. The generated numeric solutions and time to convergence are evaluated to those generated by POST for the purpose of comparison to an established solution method. DIDO⁵⁻⁹ also implements the pseudospectral method; however, GPOCS's implementation of phases is more compatible with interior point constraints, such as waypoints.

II. Optimization Methods

As stated in the introduction, several numerical techniques exist to solve constrained two point boundary value problems cast as hypersonic vehicle trajectory problems. This section will briefly introduce the numeric optimization techniques used in both POST and GPOCS.

II.A. Optimization in POST

The optimization method available in POST is the accelerated projected gradient method (PGA). The PGA algorithm is an iterative technique designed to solve a general class of nonlinear programming problems. PGA uses a cost function and constraint gradient information in place of a multidimensional optimization problem by a set of equivalent one dimensional searches. With this approach, the initial function of the PGA algorithm is to ensure constraint satisfaction, however the terminal phase of the optimization primarily ensures a reduction in the cost function. As with the case of many optimization approaches that rely on gradient information to arrive at a global minimum, shallow gradients can lead to long convergence times or fail to converge altogether. One additional problem with this optimization method is that all constraints must be considered simultaneously during the solution, which can lead to non-convergence in the case of a highly constrained problem.

II.B. Optimization in GPOCS

GPOCS uses the pseudospectral optimization method to converge to a minimal cost of a two-point boundary value problem. As stated by Jorris,^{10,11} the purpose of pseudospectral methods is to approximate the continuous solution to a set of differential equations using polynomial interpolation through discrete points or nodes. The motivation is to avoid sequential integration which can lead to divergence and may prohibit determining a solution. Lagrange, Legendre or Chebyshev polynomials, shown in Figure 1, may be used to satisfy the differential equations at a discrete number of nodes N . Computing the solution at the nodes is also termed collocation. These collocation techniques satisfy all the nodes simultaneously, thus avoiding the pitfalls of integration, especially the forward and backward integration within the shooting method. To ensure computational accuracy of the solution derived using this method, the spacing of the nodes is of critical importance. While equally spaced nodes are the simplest approach, the polynomial interpolation will lead to large errors as the number of nodes is increased. To avoid this phenomenon, known as *Runge Phenomenon*, Chebyshev point placement as defined in equation 1 may be used to distribute the nodes. The roots of the Legendre polynomials, or Gauss points, may also be used. The use of these non-uniformly spaced points allows for increased polynomial interpolation accuracy as the

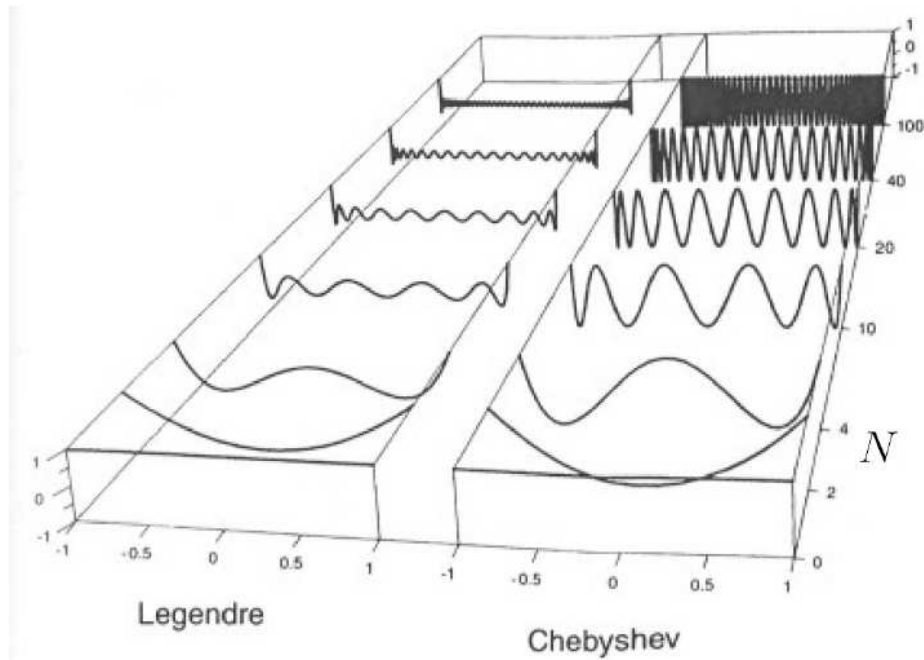


Figure 1. Comparison of Legendre and Chebyshev Polynomials.¹²

number of nodes increases.

$$x_j = \cos\left(\frac{j\pi}{N}\right), \quad j = 0, 1, \dots, N \quad (1)$$

For example, the benefit of using Chebyshev node spacing over equal spacing is depicted in Figure 2. One area of concern is that the midpoint regions along a trajectory can have relatively low node density, however this can be addressed through the use of *phases*. The term *phases* refers to inserting intermediate events into the entire span of nodes. These additional nodes create interior boundary conditions by creating new internal endpoints. This approach has the benefit of adding a higher density of nodes in regions that may otherwise have relatively low node density, which increases solution accuracy. In practice, this ability to segment the solution of a set of differential equations into phases allows greater freedom in defining a highly constrained boundary value problem. A more detailed explanation of this optimization technique is covered in Appendix B.

III. Methodology

This section briefly describes the methodology used in this paper to derive a technique that converges to a merit optimal solution. The derived method has been set up to ensure

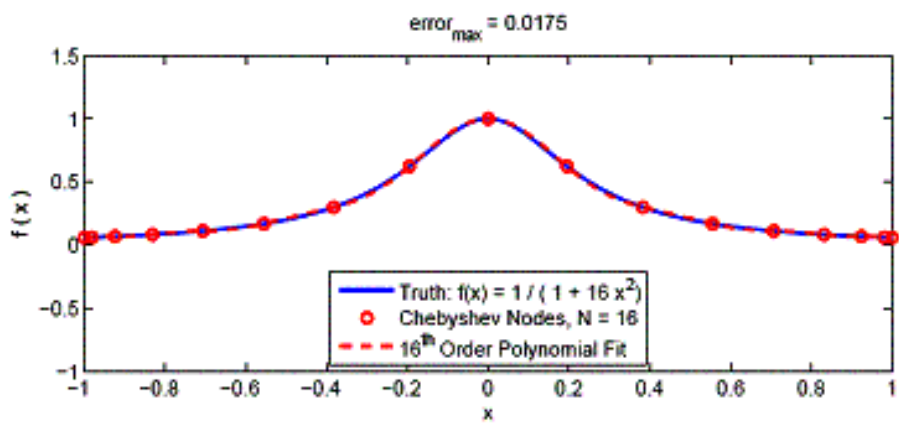
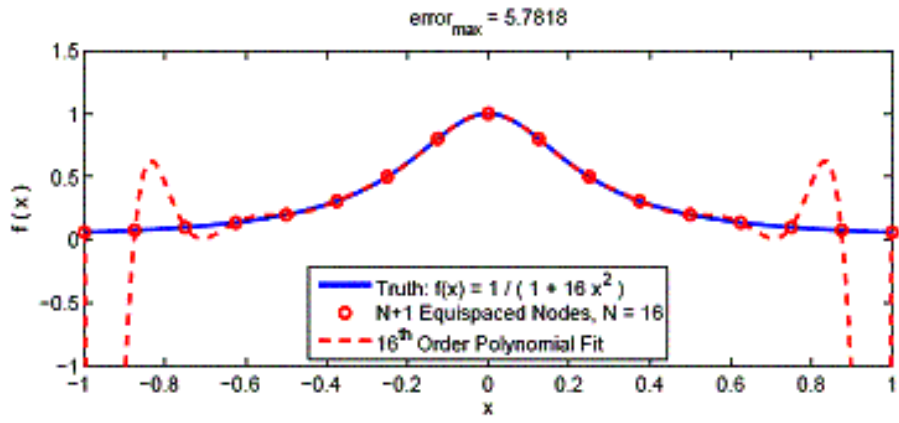


Figure 2. Demonstration of Runge Phenomenon with Equally Space Nodes.¹⁰

satisfaction of waypoint and no-fly zone constraints while requiring minimal computational time. The trajectory is constrained by the equations of motion, intermediate waypoint and no-fly zone constraints, and bank angle and lift control limitations. As a note, the bank angle control may be limited by structural loads, controllability, or heating constraints. The limitation on bank angle translates to a minimum turn radius to transition from one waypoint or no-fly zone to the next, while the coefficient of lift is used to modulate the rate of descent. Two dimensional analysis¹⁰ demonstrated the use of a geometric solution as an initial guess to the dynamic optimization technique. The work herein expands upon this previous research¹¹ to include a full three dimensional environment incorporating the earth's rotation. This expansion from a 2 dimensional to 3 dimensional environment allows for a more realistic representation of hypersonic vehicle equations of motion.

III.A. Assumptions

The following assumptions are made to scope the research effort:

1. The waypoints are specified in the desired sequence.
2. Inner-loop control is available. Only the outer-loop or trajectory generation is addressed.
3. Waypoints are sufficiently spaced such that no two are within the turn radius of the vehicle.
4. The no-fly zones are specified as elliptical exclusion zones, radiating from the center of the Earth.

III.B. Analysis

The dimensional equations of motion for an atmospheric reentry vehicle about a spherical, rotating Earth, as described by Vinh,¹³ with coefficient of lift (C_L) and coefficient of drag (C_D) are used to describe the reentry trajectory. As a note, the subscript d denotes dimensional, all angles remain in radians, and thrust is assumed zero as vehicle considered in this work is a glide vehicle. Additionally, terms denoted by a 'hat', \hat{x} , denote a non-dimensional representation of a state variable. For reference, the angles used in the equations of motion are displayed in Figure 3.

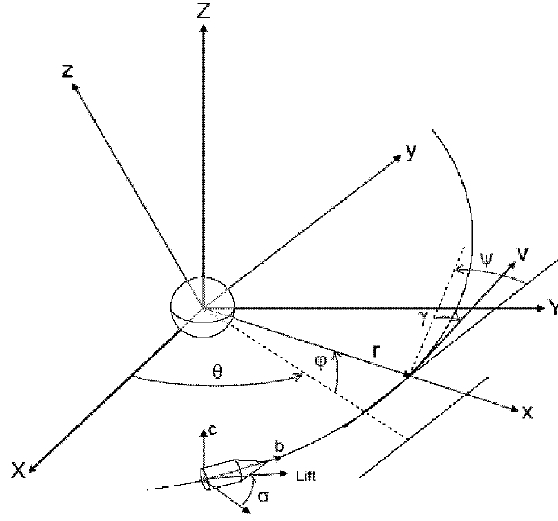


Figure 3. Spherical Coordinates for Atmospheric Flight: longitude θ , latitude ϕ , heading angle ψ , flight path angle γ , and bank angle σ

First, the dimensional kinematic and dynamic equations of motion are presented in equation 2 where ω_e is the angular velocity of earth's rotation.

$$\begin{aligned}
 \dot{r}_d &= V_d \sin \gamma \\
 \dot{\theta} &= \frac{V_d \cos \gamma \cos \psi}{r_d \cos \phi} \\
 \dot{\phi} &= \frac{V_d \cos \gamma \sin \psi}{r_d} \\
 \dot{V}_d &= \frac{-D_d}{m_d} - g_d \sin \gamma + r_d \omega_e^2 \cos \phi [\cos \phi \sin \gamma - \sin \phi \sin \psi \cos \gamma] \\
 \dot{\gamma} &= \frac{1}{V_d} \left[\frac{L_d}{m_d} \cos \sigma - g_d \cos \gamma + \frac{V_d^2}{r_d} \cos \gamma \right] \\
 &\quad + 2V_d \omega_e \cos \phi \cos \psi + r_d \omega_e^2 \cos \phi [\cos \phi \cos \gamma - \sin \phi \sin \psi \sin \gamma] \\
 \dot{\psi} &= \frac{1}{V_d} \left[\frac{L_d \sin \sigma}{m_d \cos \gamma} - \frac{V_d^2}{r_d} \cos \gamma \cos \psi \tan \phi + 2V_d \omega_e [\sin \psi \cos \phi \tan \gamma - \sin \phi] \right. \\
 &\quad \left. - \frac{r_d \omega_e^2}{\cos \gamma} \sin \phi \cos \phi \cos \psi \right] \tag{2}
 \end{aligned}$$

For the purpose of optimization, the equations in 2 are normalised so that a change in one unit of each state element is approximately of equal significance.¹⁴ These equations can be

non-dimensionalized and simplified using the variables in Eq. (3).^{13,15}

$$\begin{aligned}
\tau &= \frac{t}{\sqrt{r_0/g_0}} \\
\hat{r} &= \frac{r_d}{r_0} \\
g_d &= g_0 \left(\frac{r_0}{r_d} \right)^2 = \frac{g_0}{r^2} \text{ thus } g_0 = g_s \left(\frac{R_\oplus}{r_0} \right)^2 \\
\hat{V} &= \frac{V_d}{\sqrt{g_0 r_0}} \\
\hat{D} &= \frac{D_d}{\sqrt{g_0 m_d}} \\
\hat{L} &= \frac{L_d}{\sqrt{g_0 m_d}} \\
\rho &= \rho_0 e^{-\beta r_0 h}
\end{aligned} \tag{3}$$

The control variables are bank angle (σ) and the angle of attack (α), which ultimately regulates the lift and drag terms in equation 2. The resulting non-dimensional equation of motion are:

$$\begin{aligned}
\dot{\hat{r}} &= \hat{V} \sin \gamma \\
\dot{\hat{\theta}} &= \frac{\hat{V} \cos \gamma \cos \psi}{\hat{r} \cos \phi} \\
\dot{\hat{\phi}} &= \frac{\hat{V} \cos \gamma \sin \psi}{\hat{r}} \\
\dot{\hat{V}} &= -\hat{D} - \frac{\sin \gamma}{\hat{r}^2} + \hat{r} \omega_e^2 \cos \phi [\cos \phi \sin \gamma - \sin \phi \sin \psi \cos \gamma] \\
\dot{\hat{\gamma}} &= \frac{1}{\hat{V}} \left[\hat{L} \cos \sigma - \frac{\cos \gamma}{\hat{r}^2} + \frac{\hat{V}^2}{\hat{r}} \cos \gamma \right] \\
&\quad + 2\hat{V} \omega_e \cos \phi \cos \psi + \hat{r} \omega_e^2 \cos \phi [\cos \phi \cos \gamma - \sin \phi \sin \psi \sin \gamma] \\
\dot{\hat{\psi}} &= \frac{1}{\hat{V}} \left[\frac{\hat{L} \sin \sigma}{\cos \gamma} - \frac{\hat{V}^2}{\hat{r}} \cos \gamma \cos \psi \tan \phi + 2\hat{V} \omega_e [\sin \psi \cos \phi \tan \gamma - \sin \phi] \right. \\
&\quad \left. - \frac{\hat{r} \omega_e^2}{\cos \gamma} \sin \phi \cos \phi \cos \psi \right]
\end{aligned} \tag{4}$$

The atmospheric model used in this work was based on the U.S. Standard Atmosphere in 1976,^{16,17} with an extended altitude range of 1000km. Additionally, a spherical earth is considered in this work and thus results in a Newtonian, or inverse square law, gravity field.

IV. Results

The equations presented in the previous section are used to replicate generic hypersonic vehicle simulation results derived from Program to Optimize Simulated Trajectories (POST).^{18,19} The constant speed/altitude 2-D optimal solution was previously presented¹⁰ and derived using the discontinuous costate dynamic optimization method.²⁰ The same technique will now be applied to the 3-dimensional spherical Earth problem.

This section compares the results for several simulated 3-dimensional optimal trajectories as calculated by both POST and GPOCS. A set of desired mission profiles are established to use as a common comparison between the two methods. The missions range in constraint complexity, beginning with a benign constraint case and ending with a heavily constrained mission profile. The desired trajectories consist several constraints, which include control, heating, altitude, waypoint, and flight restriction zone constraints. The results of this analysis compare and contrast the effectiveness of the optimization methods in both POST and GPOCS to arrive at an optimal solution for each of the constrained mission profiles. The results in this section provide insight into the advantages and disadvantages in using different optimization methods for a range of mission complexities. Three comparisons make the overall evaluation of the two methods; the first to compare the underlying system dynamics of the two methods, the second to evaluate a simple max range comparison, and the final to compare a heavily constrained trajectory. The evaluation will begin with the first comparison to evaluate the system dynamics.

IV.A. Dynamics Comparison

The first comparison focuses on evaluating the basic dynamics, atmospheric model, and gravity model between POST and GPOCS. This comparison is setup to ensure subsequent comparisons are made using identical system dynamics, atmospheric model, and gravity model. This comparison also includes an evaluation between the implicit and explicit integration methods used in GPOCS and POST, respectively. This is to ensure the integration methods deliver identical results for an identical problem formulation. As stated earlier, the extended US76 atmosphere and Newtonian gravity field is used in both GPOCS and POST. To ensure identical dynamics setups a simple open loop, non optimised trajectory was integrated forward in time using a single fixed angle of attack and bank angle in both POST and GPOCS. This test resulted in identical trajectories between POST and GPOCS. As a note, this comparison used the Runge-Kutta fourth order integration method¹⁹ for both POST and the dynamics used in GPOCS. GPOCS, however, used an implicit integration method, as discussed earlier. Therefore, before any comparison in optimization was to be done, a

comparison of the separate integration methods was performed. The initial conditions and results of such comparison are presented in Figures 4 and 5. These results indicated the implicit and explicit integration methods of POST and GPOCS, respectively, produced identical trajectory results. As a note, this test used open loop, non-optimised trajectories, with fixed angles of attack of 10 degrees and a bank angle of 60 degree.

Variable	POST	SPOCS	Units
Altitude	350000	350000	ft
Radius	21275646	21275646	ft
Earth Radius	6378.137	6378.137	km
Earth Rotate	0.0041780741	0.0041780741	deg/sec
Latitude	2.5200727e-015	2.5200727e-015	deg
Longitude	3.1679632	3.1679632	deg
Velocity	14999.225	15000	ft/sec
Gamma	-3.0002544	-3.0002544	deg
Heading	90	90	deg from N
Ref Area (S)	749.9952	750	in ²
Weight	2000	2000	lbs
:-nose	1.0671966	1.0671966	feet
Time/Nodes	59	143	integer

Figure 4. Initial Conditions of Integration Method Comparison

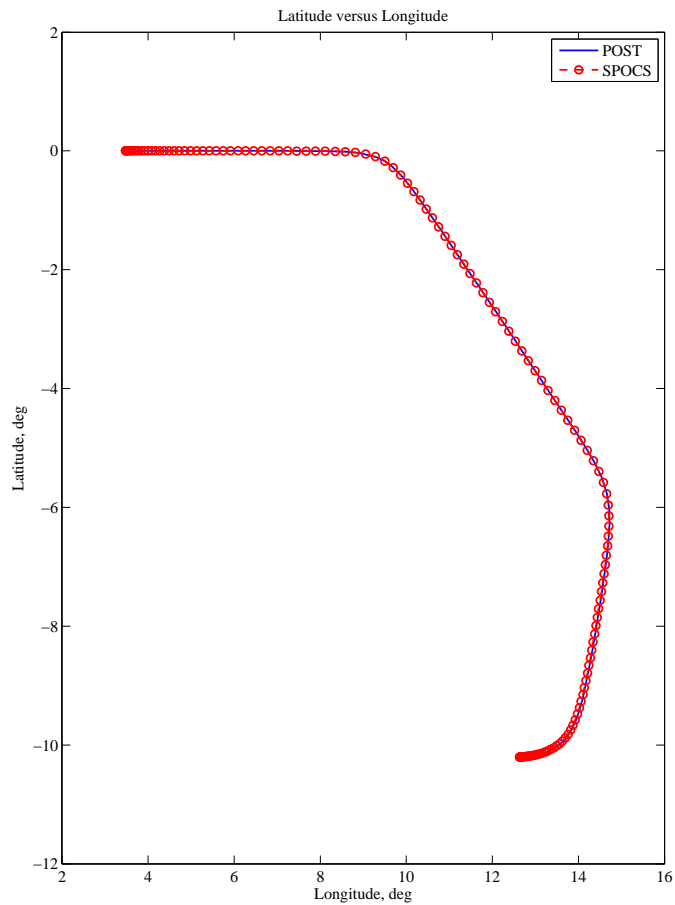


Figure 5. Trajectory Comparison of Integration Method Comparison

IV.B. Basic Optimization Comparison

The second set of comparisons involved an evaluation of the optimization methods in both GPOCS and POST. For this, a simple maximum downrange trajectory optimization was performed. The first trajectory to compare with the pseudo-spectral method was a straight gliding trajectory meeting the requirements of the DARPA FALCON program²¹ (ref: 9000nm glide range) for a 2000lb high lift hypersonic glide vehicle. The description of this vehicle is outlined in Appendix A. For the POST trajectory, three angles of attack were used to control the glide profile and allow for constraints on altitude if desired: the first AOA during reentry determines the depth into the atmosphere the hypersonic vehicle reenters before ‘skipping’ up into a glide, the second AOA determines how high the vehicle ‘skips’, and the third is held constant for the remainder of the trajectory causing a ‘phugoid’ or ‘skipping’ trajectory. The initial conditions (or reentry conditions) were found given the vehicle weight and range requirement. The resulting reentry velocity and flight path angle were consistent with the original DARPA FALCON concept: launching a 2000lb HTV-1 from

a SpaceX Falcon 1 launch vehicle. The three initial guesses for angles of attack were based on experience. Once the initial conditions and guesses were set, non-optimized trajectories using constant alpha and then constant bank angle were run to validate the equations of motion in the pseudo-spectral model. To ensure simplicity in this evaluation the only criteria that was evaluated was imply the cost of the final longitude value, with the only constraints being a minimum altitude value of 27.4 kilometers, or 90k feet, and a final time of 3063 seconds, that being the run time of the POST trajectory. The maximum time was chosen to more closely align the GPOCS results to that of the POST run. The initial conditions, altitude, attained down range values, and angle of attack comparison plots are presented in Figures 6,7,8, and 9.

Variable	POST	SPOCS	Units
Altitude	350000	350000	ft
Radius	21275646	21275646	ft
Earth Radius	6378.137	6378.137	km
Earth Rotate	0.0041780741	0.0041780741	deg/sec
Latitude	1.2127847e-014	1.2127847e-014	deg
Longitude	16.951296	16.951296	deg
Velocity	20998.56	21000	ft/sec
gamma	-3	-3	deg
Heading	90	90	deg from N
Ref Area (S)	749.9952	750	in ²
Weight	2000	2000	lbs
i-nose	1.0671966	1.0671966	feet
Times/Nodes	290	107	integer

Figure 6. Initial Conditions of the First Optimization Comparison

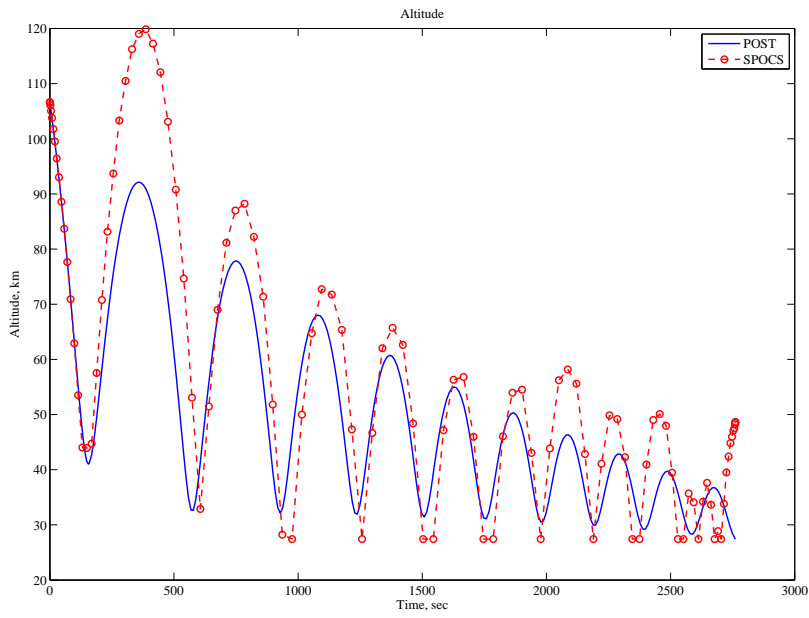


Figure 7. Altitude Comparison of the First Optimization Comparison

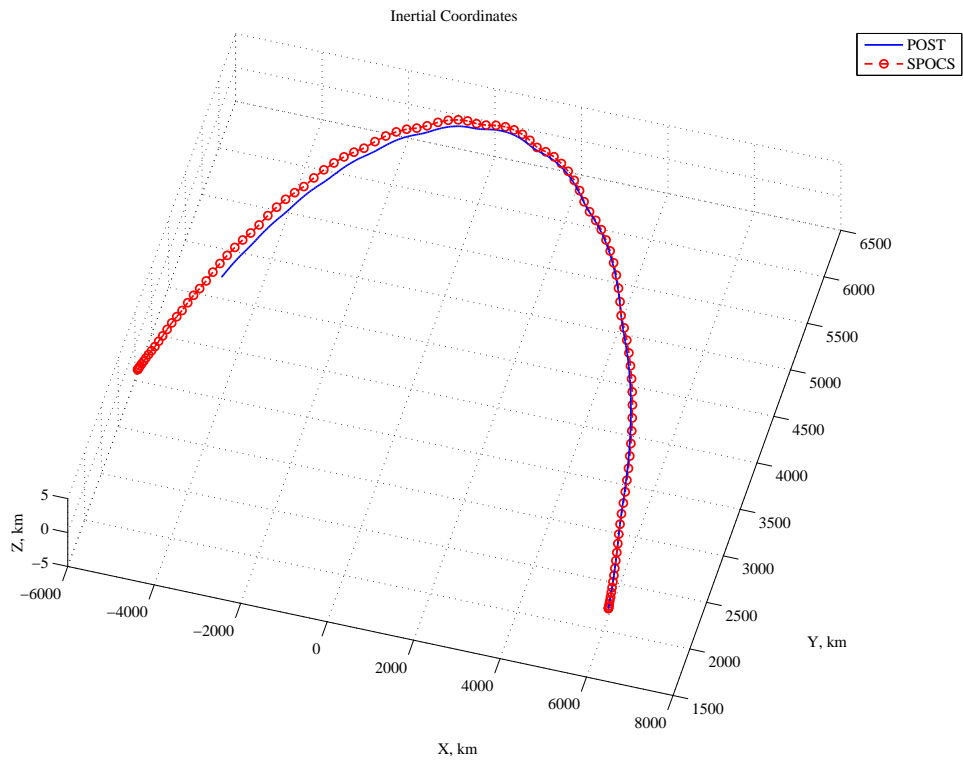


Figure 8. Range Comparison of the First Optimization Comparison

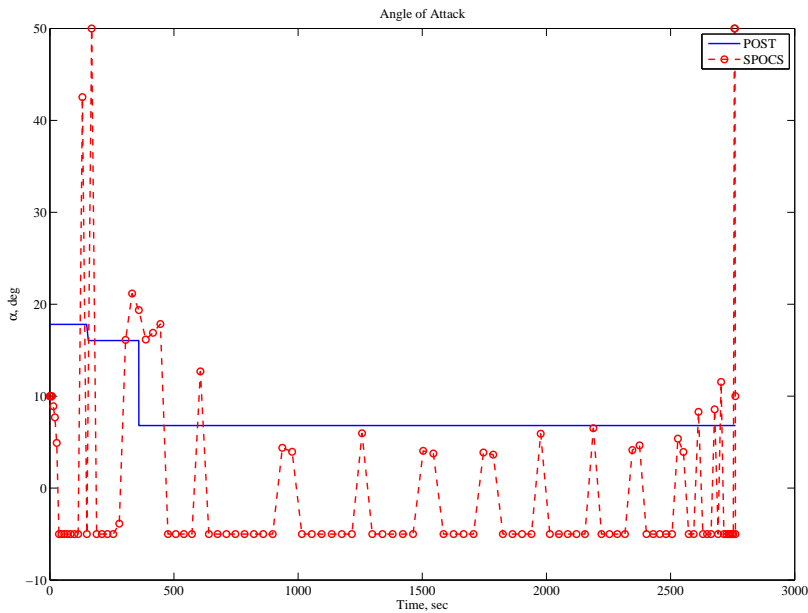


Figure 9. Angle of Attack Comparison of the First Optimization Comparison

The greatest distinction revealed from this comparison was the flexibility in available control afforded to the user in GPOCS, as seen in Figure 9 . Herein, the user defines a control input vector containing the value of each control at every node along the trajectory. This is contrasted with POST, where the user can only specify discrete control inputs which are then optimised to attain the maximum down range value. Consequently, finer control variability in GPOCS has resulted in a greater downrange value, as seen in Figure 8. The next comparison will present a more constrained problem to compare and contrast.

IV.C. Complex Optimization Comparison

In this comparison, POST was set up to fly a hypersonic glide trajectory following a ballistic reentry with fixed reentry conditions. Here, a problem was set up to launch a hypersonic glide vehicle from Cape Canaveral to the Persian Gulf, flying over the Mediterranean Sea with minimal overflight of land. This was done by specifying a waypoint at the Strait of Gibraltar and two no-fly zones, one in North Africa and one in South-central Europe. POST simulated the glide from reentry so an arbitrary reentry point (see output files) was determined as an initial condition. The reentry velocity and flight path angle were kept the same as the prior case, but reentry azimuth was allowed to vary assuming a booster would tailor its profile to meet the desired end conditions. The trajectory was optimized for maximum final altitude, terminating at a set velocity. This forced POST to

converge to a solution that would conserve the most energy, i.e. not waste energy through excessive maneuvering. However, significant maneuvering was required to hit the waypoint and avoid the no-fly zones. Considering that reentry azimuth could vary, this required three bank maneuvers for each geographic constraint and a fourth bank maneuver to straighten the glide before the terminal condition. Bank angles, bank duration, and time between turns were set up as independent variables to go along with the three angles of attack from before. Dependent variables were reentry angle, and the geographic constraints of the waypoint and no-fly zones. These constraints were defined by using ‘tracking stations’ in POST and applying limits to ‘slant range’ either forcing the trajectory towards or away from the particular station.

To set up a problem such as this in POST, one cannot apply all the constraints at once and expect POST to come to a solution. The problem must be built up as constraints are applied one at a time. Using the trajectory from the pseudo-spectral validation and adding four banking maneuvers, one could quickly converge to a solution that when projected on a Mercator Projected map, looks close to the desired solution . However, the guesses for angles of attack, bank angles, and durations were all based on experience and did not taking into account the geographic constraints. This ‘first-cut’ is useful however for generating new independent variables to be used once these constraints are applied. Additionally by outputting the slant ranges for each of the three tracking stations, even though they are not yet used for constraints, one can make changes in the independent variables to observe how the slant ranges change to better determine the first guess once the constraints are applied.

Even though the above described trajectory is close to the solution, POST cannot yet handle all three geographic constraints being applied at once. Therefore the problem added the complexity of the waypoint located at the Strait of Gibraltar and the user could continue to monitor the slant ranges to the other two tracking stations. This process continued, adding one geographic constraint at a time until all constraints were applied and the problem could be optimized. Even then, POST was unable to converge on a ‘best’ solution although all the constraints were met.

Once the first trajectory to the Persian Gulf was found using POST each geographic constraint was applied one at a time. The geographic constraints were based on tracking stations with slant ranges used to either keep the trajectory near or far from the stations. Because of the narrow width of the Strait of Gibraltar, the tolerance for the waypoint was first a quarter nautical mile, but this prevented POST from converging on a solution. The tolerance was then relaxed to one nautical mile and POST was then able to converge on a solution. The no-fly zones were defined to avoid overflight of land in North Africa and South-central Europe, so a minimum distance to each tracking station was defined. Here,

the tolerance on each slant range had to be relaxed to five significant digits , as the slant range is measured in feet. This translated to approximately one a two-thirds nautical miles.

The first trajectory to the Persian Gulf without any geographic constraints took a CPU time of .4 seconds . Applying the first waypoint increased the CPU time to .5 sec . The first no-fly zone made the CPU time at .6 sec. This case reached the iteration limit without finding a solution. However, by noting the errors on the constraints, the user was able to modify the independent variables to make a reasonable first guess with all geographic constraints applied. Even so, this case also ran to the iteration limit without converging on a solution. In this case CPU time was still .6 seconds. In all, this process took an experienced POST user (with experience modeling hypersonic glide trajectories, enabling educated first guesses) a day and a half, running POST approximately 30 times with up to 50 iterations each.

In comparison, the method to generate the mission described above using GPOCS was significantly easier. The overall trajectory as compared to POST is presented in Figure 10.



Figure 10. Initial Conditions of the Final Optimization Comparison

Upon the user defining the waypoint, being the end of the first phase, and the no fly zones as the path constraints the trajectory is ready to be run. Simply put, no iterative method is necessary to generate the trajectory as in the case of POST. The results of the trajectory comparison is seen in Figures 11 through 15

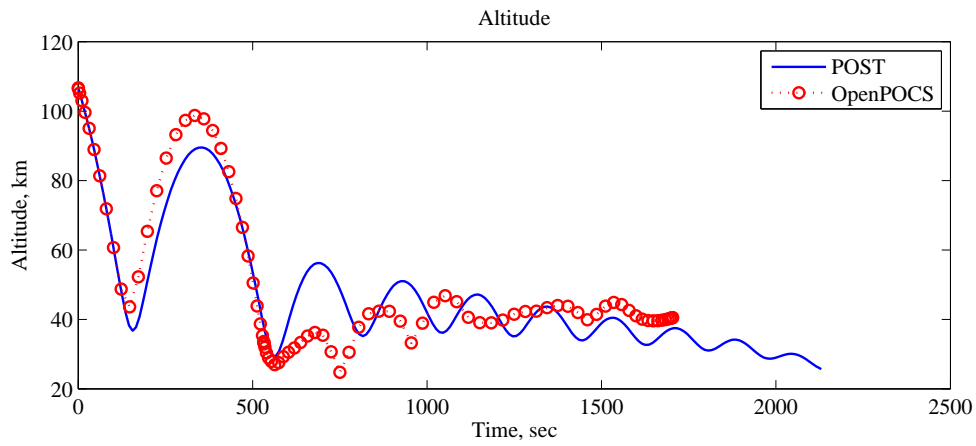


Figure 11. Altitude Comparison of the Final Optimization Comparison

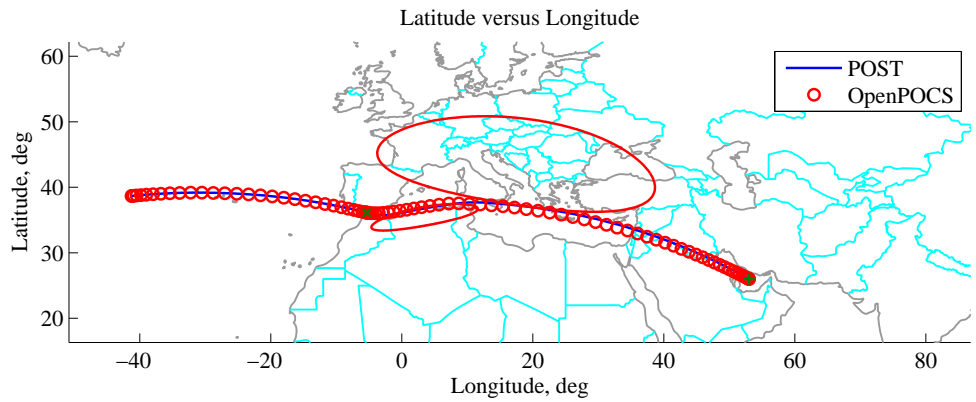


Figure 12. Latitude and Longitude of the Final Optimization Comparison

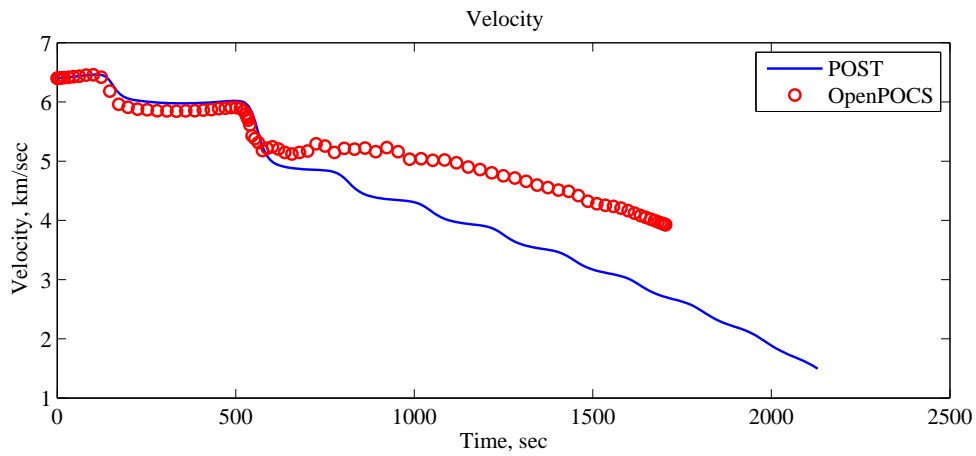


Figure 13. Velocity of the Final Optimization Comparison

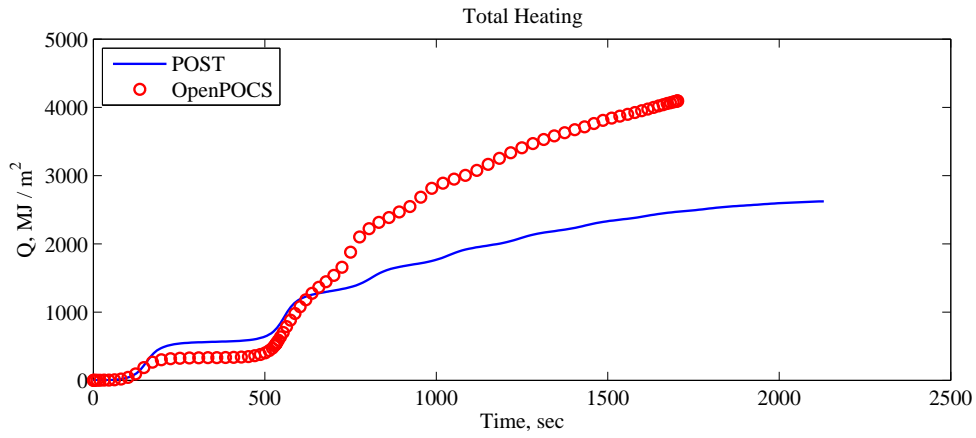


Figure 14. Total Heat of the Final Optimization Comparison

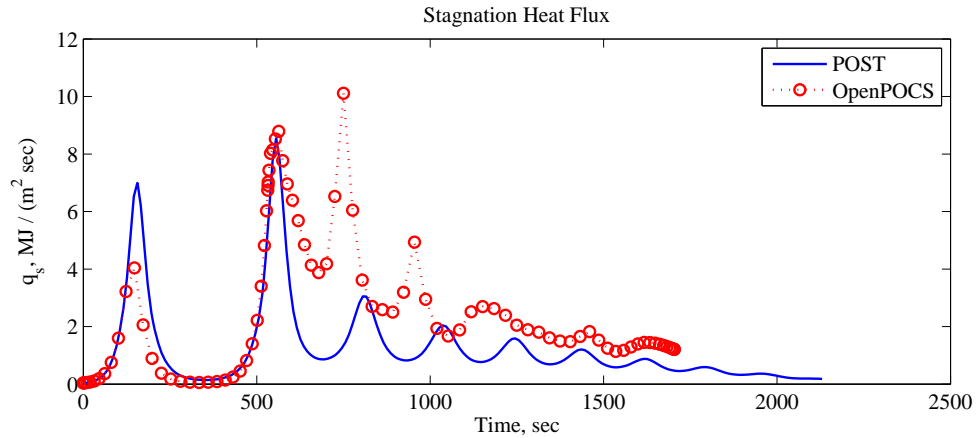


Figure 15. Peak Heating of the Final Optimization Comparison

V. Conclusion

This paper presents an example of employing the Gauss Pseudospectral Optimization method in optimal trajectory generation of a hypersonic glide vehicle. A brief description of the implicit optimization method used in the Pseudospectral method is discussed and contrasted with the method used in POST. A series of comparison optimal trajectories are presented and reviewed. The comparisons reveal GPOCS generated trajectories produce similar results to those of POST. However, the iterative approach commonly used in POST is not necessary to successfully generate a complex trajectory in GPOCS.

VI. Acknowledgments

The research presented in this document is sponsored by the hours of donated time by otherwise extortionately employed officers in the United States Air Force.

VII. Appendix

A. Hypersonic Vehicle Aerodynamic Data

The following is taken from¹⁸ and is used to create a Mach independent model for use in this research.

Table A.1. High Lift Hypersonic Glide Vehicle Aero Data Base

Lift to Drag Ratio (L/D)							
AOA	Mach 3.5	Mach 5	Mach 8	Mach 10	Mach 15	Mach 20	Mach 23
10°	2.2000	2.5000	3.1000	3.5000	3.3846	3.2692	3.2000
15°	2.5000	2.6616	2.9846	3.2000	3.0846	2.9692	2.9000
20°	2.2000	2.3616	2.6846	2.9000	2.7846	2.6692	2.6000
Coefficient of Lift (C_L)							
AOA	Mach 3.5	Mach 5	Mach 8	Mach 10	Mach 15	Mach 20	Mach 23
10°	0.4500	0.4250	0.4000	0.3800	0.3700	0.3600	0.3500
15°	0.7400	0.7000	0.6700	0.6300	0.6000	0.5700	0.5570
20°	1.0500	1.0000	0.9500	0.9000	0.8500	0.8000	0.7800
Coefficient of Drag (C_D)							
AOA	Mach 3.5	Mach 5	Mach 8	Mach 10	Mach 15	Mach 20	Mach 23
10°	0.2045	0.1700	0.1290	0.1090	0.1090	0.1090	0.1090
15°	0.2960	0.2630	0.2240	0.1970	0.1950	0.1920	0.1920
20°	0.4770	0.4230	0.3540	0.3100	0.3050	0.3000	0.3000

HGV-H Aero Reference Area $S_{ref} = 750 \text{ in}^2$

HGV-H Mass $m = 2000 \text{ lbs} = 907.186 \text{ kg}$ (assuming $g = 32.174 \text{ ft/s}^2$)

B. Gauss Pseudospectral Method Exposition

For completeness, an introduction to the Gauss Pseudospectral Method (GPM), which is the basis for the software package used in this research, is presented below. The GPM is an orthogonal collocation method where the collocation points are the *Legendre-Gauss* (LG) points. The description herein is a compilation from^{1,22-26} which is based on.^{27,28} Additional implementation methods are in.^{26,29-31}

B.I. Continuous Bolza Problem

The dynamic optimization problem is restated here with the transformation of the independent variable t :

$$t = \frac{t_f - t_0}{2}\tau + \frac{t_f + t_0}{2} \quad (\text{B.1})$$

The optimal control problem is to determine the state, $\mathbf{x}(\tau) \in \mathbb{R}^n$, control, $\mathbf{u}(\tau) \in \mathbb{R}^m$, initial time, t_0 , and final time, t_f , that minimizes the cost functional:

$$J = \phi(\mathbf{x}(-1), t_0, \mathbf{x}(1), t_f) + \frac{t_f - t_0}{2} \int_{-1}^1 L(\mathbf{x}(\tau), \mathbf{u}(\tau), \tau; t_0, t_f) d\tau \quad (\text{B.2})$$

subject to the constraints

$$\frac{d\mathbf{x}}{d\tau} = \frac{t_f - t_0}{2} f(\mathbf{x}(\tau), \mathbf{u}(\tau), \tau; t_0, t_f) \quad (\text{B.3})$$

$$\psi(\mathbf{x}(-1), t_0, \mathbf{x}(1), t_f) = 0 \quad (\text{B.4})$$

$$C(\mathbf{x}(\tau), \mathbf{u}(\tau), \tau; t_0, t_f) \leq 0 \quad (\text{B.5})$$

Herein, the optimal control problem of Eqs. (B.2-B.5) is called the *continuous Bolza problem*.

B.II. Gauss Pseudospectral Discretization of Continuous Bolza Problem

The direct approach to solving the continuous Bolza optimal control problem of Sec. B.I is to discretize and transcribe Eqs. (B.2-B.5) to a nonlinear programming problem (NLP). The Gauss pseudospectral method, like Legendre and Chebyshev methods, is based on approximating the state and control trajectories using interpolating polynomials. The state is approximated using a basis of $N + 1$ Lagrange interpolating polynomials, \mathcal{L} .

$$\mathbf{x}(\tau) \approx \mathbf{X}(\tau) = \sum_{i=0}^N \mathbf{X}(\tau_i) \mathcal{L}_i(\tau) \quad (\text{B.6})$$

where $\mathcal{L}_i(\tau)(i = 0, \dots, N)$ are defined as

$$\mathcal{L}_i(\tau) = \prod_{j=0, j \neq i}^N \frac{\tau - \tau_j}{\tau_i - \tau_j} \quad (\text{B.7})$$

Additionally, the control is approximated using a basis of N Lagrange interpolating polynomials $\mathcal{L}_i^*(\tau), (i = 1, \dots, N)$ as

$$\mathbf{u}(\tau) \approx \mathbf{U}(\tau) = \sum_{i=1}^N \mathbf{U}(\tau_i) \mathcal{L}_i^*(\tau) \quad (\text{B.8})$$

where

$$\mathcal{L}_i^*(\tau) = \prod_{j=1, j \neq i}^N \frac{\tau - \tau_j}{\tau_i - \tau_j} \quad (\text{B.9})$$

It can be seen from Eqs. (B.7) and (B.9) that $\mathcal{L}_i(\tau)(i = 0, \dots, N)$ and $\mathcal{L}_i^*(\tau)(i = 1, \dots, N)$ satisfy the properties

$$\mathcal{L}_i(\tau_j) = \begin{cases} 1 & , \quad i = j \\ 0 & , \quad i \neq j \end{cases} \quad \text{and} \quad \mathcal{L}_i^*(\tau_j) = \begin{cases} 1 & , \quad i = j \\ 0 & , \quad i \neq j \end{cases} \quad (\text{B.10})$$

Differentiating the expression in Eq. (B.6) produces

$$\dot{\mathbf{x}}(\tau) \approx \dot{\mathbf{X}}(\tau) = \sum_{i=0}^N \mathbf{X}(\tau_i) \dot{\mathcal{L}}_i(\tau) \quad (\text{B.11})$$

The derivative of each Lagrange polynomial at the LG points can be represented in a differential approximation matrix, $D \in \mathbb{R}^{N \times N+1}$. The elements of the differential approximation matrix are determined offline as follows:

$$D_{ki} = \dot{\mathcal{L}}_i(\tau_k) = \sum_{i=0}^N \frac{\prod_{j=0, j \neq i, l}^N (\tau_k - \tau_j)}{\prod_{j=0, j \neq i}^N (\tau_i - \tau_j)} \quad (\text{B.12})$$

where $k = 1, \dots, N$ and $i = 0, \dots, N$. The dynamic constraint is transcribed into algebraic constraints via the differential approximation matrix as follows:

$$\sum_{i=0}^N D_{ki} \mathbf{X}_i - \frac{t_f - t_0}{2} f(\mathbf{X}_k, \mathbf{U}_k, \tau_k; t_0, t_f) = 0 \quad (k = 1, \dots, N) \quad (\text{B.13})$$

where $\mathbf{X}_k \equiv \mathbf{X}(\tau_k) \in \mathbb{R}^n$ and $\mathbf{U}_k \equiv \mathbf{U}(\tau_k) \in \mathbb{R}^m$ ($k = 1, \dots, N$). Note that the dynamic constraint is collocated only at the LG points and *not* at the boundary points (this form of collocation differs from other well known pseudospectral methods^{31,32}). Additional variables in the discretization are defined as follows: $\mathbf{X}_0 \equiv \mathbf{X}(-1)$, and $\mathbf{X}_f \equiv \mathbf{X}(1)$, where \mathbf{X}_f is defined in terms of \mathbf{X}_k , ($k = 0, \dots, N$) and $\mathbf{U}(\tau_k)$ ($k = 1, \dots, N$) via the Gauss quadrature.³³

$$\mathbf{X}_f \equiv \mathbf{X}_0 + \frac{t_f - t_0}{2} \sum_{k=1}^N w_k f(\mathbf{X}_k, \mathbf{U}_k, \tau_k; t_0, t_f) \quad (\text{B.14})$$

The continuous cost function of Eq. (B.2) is approximated using a Gauss quadrature³³ as

$$J = \phi(\mathbf{X}_0, t_0, \mathbf{X}_f, t_f) + \frac{t_f - t_0}{2} \sum_{k=1}^N w_k L(\mathbf{X}_k, \mathbf{U}_k, \tau_k; t_0, t_f) : \quad (\text{B.15})$$

where w_k are the Gauss weights. The boundary constraint of Eq. (B.4) is expressed as

$$\psi(\mathbf{X}_0, t_0, \mathbf{X}_f, t_f) = 0 \quad (\text{B.16})$$

Furthermore, the path constraint of Eq. (B.5) is evaluated at the LG points as

$$C(\mathbf{X}_k, \mathbf{U}_k, \tau_k; t_0, t_f) \leq 0 \quad (k = 1, \dots, N) \quad (\text{B.17})$$

The cost function of Eq. (B.15) and the algebraic constraints of Eqs. (B.13), (B.14), (B.16), and (B.17) define an NLP whose solution is an approximate solution to the continuous Bolza problem. Finally, it is noted that the above discretization can be employed in multiple-phase problems by transcribing the problem in each phase using the above discretization and connecting the phases by *linkage* constraints:

$$\mathbf{P}^{(s)}(\mathbf{x}^{(p_l^s)}(t_f), t_f^{(p_l^s)}; \mathbf{q}^{(p_l^s)}, \mathbf{x}^{(p_u^s)}(t_0), t_0^{(p_u^s)}; \mathbf{q}^{(p_u^s)}) = 0, \quad (p_l, p_u \in [1, \dots, P], s = 1, \dots, L_p) \quad (\text{B.18})$$

where $\mathbf{x}^{(p)}(t) \in \mathbb{R}^{n_p}$, $\mathbf{u}^{(p)}(t) \in \mathbb{R}^{m_p}$, $\mathbf{q}^{(p)} \in \mathbb{R}^{q_p}$, and $t \in \mathbb{R}$ are, respectively, the state, control, static parameters, and time in phase $p \in [1, \dots, P]$, L_p is the number of phases to be linked,

$p_l^s \in [1, \dots, P]$, ($s = 1, \dots, L_p$) are the “left” phase numbers, and $p_u^s \in [1, \dots, P]$, ($s = 1, \dots, L_p$) are the “right” phase numbers. where the sum of the cost for each phase:

$$J = \sum_{p=1}^P J^{(p)} \quad (\text{B.19})$$

becomes the final cost to be minimized.

B.III. KKT Conditions of the NLP

The first-order optimality conditions (i. e. , the Karush-Kuhn-Tucker (KKT) conditions) of the NLP can be obtained using the augmented cost function or Lagrangian. The augmented cost function is formed using the Lagrange multipliers $\tilde{\Lambda}_k \in \mathbb{R}^n$, $\tilde{\mu}_k \in \mathbb{R}^c$, $k = 1, \dots, N$, $\tilde{\Lambda}_F \in \mathbb{R}^n$, and $\tilde{v} \in \mathbb{R}^q$ as

$$\begin{aligned} J_a = & \phi(\mathbf{X}_0, t_0, \mathbf{X}_f, t_f) + \frac{t_f - t_0}{2} \sum_{k=1}^N w_k L(\mathbf{X}_k, \mathbf{U}_k, \tau_k; t_0, t_f) - \tilde{v}^T \psi(\mathbf{X}_0, t_0, \mathbf{X}_f, t_f) \\ & - \sum_{k=1}^N \tilde{\mu}_k^T C(\mathbf{X}_k, \mathbf{U}_k, \tau_k; t_0, t_f) - \sum_{k=1}^N \tilde{\Lambda}_k^T \left(\sum_{i=1}^N D_{ki} \mathbf{X}_i - \frac{t_f - t_0}{2} f(\mathbf{X}_k, \mathbf{U}_k, \tau_k; t_0, t_f) \right) \\ & - \tilde{\Lambda}_F^T \left(\mathbf{X}_f - \mathbf{X}_0 - \frac{t_f - t_0}{2} \sum_{k=1}^N w_k f(\mathbf{X}_k, \mathbf{U}_k, \tau_k; t_0, t_f) \right) \end{aligned} \quad (\text{B.20})$$

The KKT conditions are found by setting equal to zero the derivatives of the Lagrangian with respect to \mathbf{X}_0 , \mathbf{X}_k , \mathbf{X}_f , \mathbf{U}_k , $\tilde{\Lambda}_k$, $\tilde{\mu}_k$, $\tilde{\Lambda}_F$, \tilde{v} , t_0 , t_f . The solution to the NLP of Sec. B.II

must satisfy the following KKT conditions:

$$\sum_{i=0}^N \mathbf{X}_i D_{ki} = \frac{t_f - t_0}{2} f_k \quad (\text{B.21})$$

$$\sum_{i=1}^N \left(\frac{\tilde{\Lambda}_i^T}{w_i} + \tilde{\Lambda}_F^T \right) D_{ki} + \tilde{\Lambda}_F^T D_{kN+1} = \frac{t_f - t_0}{2} \left(\frac{\partial L_k}{\partial \mathbf{X}_k} - \left(\frac{\tilde{\Lambda}_k^T}{w_k} + \tilde{\Lambda}_F^T \right) \frac{\partial f_k}{\partial \mathbf{X}_k} + \frac{2}{t_f - t_0} \frac{\tilde{\mu}_k^T}{w_k} \frac{\partial C_k}{\partial \mathbf{X}_k} \right) \quad (\text{B.22})$$

$$0 = \frac{\partial L_k}{\partial \mathbf{U}_k} + \left(\frac{\tilde{\Lambda}_k^T}{w_k} + \tilde{\Lambda}_F^T \right) \frac{\partial f_k}{\partial \mathbf{U}_k} - \frac{2}{t_f - t_0} \frac{\tilde{\mu}_k^T}{w_k} \frac{\partial C_k}{\partial \mathbf{U}_k} \quad (\text{B.23})$$

$$\psi(\mathbf{X}_o, t_0, \mathbf{X}_f, t_f) = 0 \quad (\text{B.24})$$

$$\tilde{\Lambda}_0^T = -\frac{\partial \phi}{\partial \mathbf{X}_0} + \tilde{\nu}^T \frac{\partial \psi}{\partial \mathbf{X}_0} \quad (\text{B.25})$$

$$\tilde{\Lambda}_F^T = \frac{\partial \phi}{\partial \mathbf{X}_f} - \tilde{\nu}^T \frac{\partial \psi}{\partial \mathbf{X}_f} \quad (\text{B.26})$$

$$-\frac{t_f - t_0}{2} \sum_{k=1}^N w_k \frac{\partial \tilde{H}_k}{\partial t_0} + \frac{1}{2} \sum_{k=1}^N w_k \tilde{H}_k = \frac{\partial \phi}{\partial t_0} - \tilde{\nu}^T \frac{\partial \psi}{\partial t_0} \quad (\text{B.27})$$

$$\frac{t_f - t_0}{2} \sum_{k=1}^N w_k \frac{\partial \tilde{H}_k}{\partial t_f} + \frac{1}{2} \sum_{k=1}^N w_k \tilde{H}_k = -\frac{\partial \phi}{\partial t_f} + \tilde{\nu}^T \frac{\partial \psi}{\partial t_f} \quad (\text{B.28})$$

$$C_k \leq 0 \quad (\text{B.29})$$

$$\tilde{\mu}_{jk} = 0, \text{ when } C_{jk} < 0 \quad (\text{B.30})$$

$$\tilde{\mu}_{jk} \leq 0, \text{ when } C_{jk} = 0 \quad (\text{B.31})$$

$$\mathbf{X}_f = \mathbf{X}_0 + \frac{t_f - t_0}{2} \sum_{k=1}^N w_k f_k \quad (\text{B.32})$$

$$\tilde{\Lambda}_F = \tilde{\Lambda}_0 + \frac{t_f - t_0}{2} \sum_{k=1}^N w_k \left(-\frac{\partial L_k}{\partial \mathbf{X}_k} - \left(\frac{\tilde{\Lambda}_k^T}{w_k} + \tilde{\Lambda}_F^T \right) \frac{\partial f_k}{\partial \mathbf{X}_k} + \frac{2}{t_f - t_0} \frac{\tilde{\mu}_k^T}{w_k} \frac{\partial C_k}{\partial \mathbf{X}_k} \right) \quad (\text{B.33})$$

where the shorthand notation $L_k \equiv L(\mathbf{X}_k, \mathbf{U}_k, \tau_k; t_0, t_f)$, $f_k \equiv f(\mathbf{X}_k, \mathbf{U}_k, \tau_k; t_0, t_f)$, $\tilde{H}_k \equiv \tilde{H}_k(\mathbf{X}_k, \tilde{\Lambda}_k, \tilde{\mu}_k, \mathbf{U}_k, \tau_k; t_0, t_f)$, and $C_{jk} \equiv C_j(\mathbf{X}_k, \mathbf{U}_k, \tau_k; t_0, t_f)$ is used. The augmented Hamiltonian, \tilde{H}_k , is defined as

$$\tilde{H}_k \equiv L_k + \left(\frac{\tilde{\Lambda}_k^T}{w_k} + \tilde{\Lambda}_F^T \right) f_k - \frac{2}{t_f - t_0} \frac{\tilde{\mu}_k^T}{w_k} C_k \quad (\text{B.34})$$

and $\tilde{\Lambda}_0$ is defined as

$$\tilde{\Lambda}_0^T = -\frac{\partial\phi}{\partial\mathbf{X}_0} + \tilde{\nu}^T \frac{\partial\psi}{\partial\mathbf{X}_0} \quad (\text{B.35})$$

Note that the sign of the $\tilde{\mu}_k^T$ term is opposite to the μ^T term; thus, the software output requires a sign change to match the analytical results presented prior to this Appendix.

B.IV. First-Order Optimality Conditions of Continuous Bolza Problem

The indirect approach to solving the continuous Bolza problem of Eqs. (B.2-B.5) in Sec. B.I is to apply the calculus of variations and Pontryagin's Maximum Principle³⁴ to obtain the first-order necessary conditions for optimality.³⁵ These variational conditions are typically derived using the augmented Hamiltonian, H , defined as

$$H(\mathbf{x}, \lambda, \mu, \mathbf{u}, \tau; t_0, t_f) = L(\mathbf{x}, \mathbf{u}, \tau; t_0, t_f) + \lambda^T(\tau)f(\mathbf{x}, \mathbf{u}, \tau; t_0, t_f) - \mu^T(\tau)C(\mathbf{x}, \mathbf{u}, \tau; t_0, t_f) \quad (\text{B.36})$$

where $\lambda(\tau) \in \mathbb{R}^n$ is the costate and $\mu(\tau) \in \mathbb{R}^c$ is the Lagrange multiplier associated with the path constraint. The continuous-time first-order optimality conditions can be shown to be

$$\frac{d\mathbf{x}}{d\tau} = \frac{t_f - t_0}{2} f(\mathbf{x}, \mathbf{u}, \tau; t_0, t_f) = \frac{t_f - t_0}{2} \frac{\partial H}{\partial \lambda} \quad (\text{B.37a})$$

$$\frac{d\lambda}{d\tau} = \frac{t_f - t_0}{2} \left(-\frac{\partial L}{\partial \mathbf{x}} - \lambda^T \frac{\partial f}{\partial \mathbf{x}} + \mu^T \frac{\partial C}{\partial \mathbf{x}} \right) = -\frac{t_f - t_0}{2} \frac{\partial H}{\partial \mathbf{x}} \quad (\text{B.37b})$$

$$0 = \frac{\partial L}{\partial \mathbf{u}} + \lambda^T \frac{\partial f}{\partial \mathbf{u}} - \mu^T \frac{\partial C}{\partial \mathbf{u}} = \frac{\partial H}{\partial \mathbf{u}} \quad (\text{B.37c})$$

$$\psi(\mathbf{x}(\tau_0), t_0, \mathbf{x}(\tau_f), t_f) = 0 \quad (\text{B.37d})$$

$$\lambda(\tau_0) = -\frac{\partial\phi}{\partial\mathbf{x}(\tau_0)} + \nu^T \frac{\partial\psi}{\partial\mathbf{x}(\tau_0)}, \quad \lambda(\tau_f) = \frac{\partial\phi}{\partial\mathbf{x}(\tau_f)} - \nu^T \frac{\partial\psi}{\partial\mathbf{x}(\tau_f)} \quad (\text{B.37e})$$

$$H(t_0) = \frac{\partial\phi}{\partial t_0} - \nu^T \frac{\partial\psi}{\partial t_0}, \quad H(t_f) = -\frac{\partial\phi}{\partial t_f} + \nu^T \frac{\partial\psi}{\partial t_f} \quad (\text{B.37f})$$

$$\mu_j(\tau) = 0, \quad \text{when } C_j(\mathbf{x}, \mathbf{u}, \tau; t_0, t_f) < 0, \quad j = 1, \dots, c \quad (\text{B.37g})$$

$$\mu_j(\tau) \leq 0, \quad \text{when } C_j(\mathbf{x}, \mathbf{u}, \tau; t_0, t_f) = 0, \quad j = 1, \dots, c \quad (\text{B.37h})$$

where $\nu \in \mathbb{R}^q$ is the Lagrange multiplier associated with the boundary condition ψ . It can be shown that the augmented Hamiltonian at the initial and final times can be written, respectively, as

$$H(t_0) = -\frac{t_f - t_0}{2} \int_{-1}^1 \frac{\partial H}{\partial t_0} d\tau + \frac{1}{2} \int_{-1}^1 H d\tau \quad (\text{B.38})$$

$$H(t_f) = \frac{t_f - t_0}{2} \int_{-1}^1 \frac{\partial H}{\partial t_f} d\tau + \frac{1}{2} \int_{-1}^1 H d\tau \quad (\text{B.39})$$

B.V. Gauss Pseudospectral Discretization Necessary Conditions

In order to discretize the variational conditions of Sec. B.IV using the Gauss pseudospectral discretization, it is necessary to form a suitable approximation for the costates. In this method, the costate, $\lambda(\tau)$, is approximated as follows:

$$\lambda(\tau) \approx \Lambda(\tau) = \sum_{i=1}^{N+1} \lambda(\tau_i) \mathcal{L}_i^\dagger(\tau) \quad (\text{B.40})$$

where $\mathcal{L}_i^\dagger(\tau)(i = 1, \dots, N + 1)$ are defined as

$$\mathcal{L}_i^\dagger(\tau) = \prod_{j=1, j \neq i}^{N+1} \frac{\tau - \tau_j}{\tau_i - \tau_j} \quad (\text{B.41})$$

It is emphasized that the costate approximation is *different* from the state approximation. In particular, the basis of the $N + 1$ Lagrange interpolating polynomials $\mathcal{L}_i^\dagger(\tau)(i = 1, \dots, N + 1)$ includes the costate at the *final* time (as opposed to the initial time which is used in the state approximation). This (non-intuitive) costate approximation is necessary in order to provide a complete mapping between the KKT conditions and the variational conditions.

Using the costate approximation of Eq. (B.40), the first-order necessary conditions of the continuous Bolza problem in Eq. (B.37) are discretized as follows. First, the state and control are approximated using Eq. (B.6) and Eq. (B.8), respectively. Next, the costate is approximated using the basis of $N + 1$ Lagrange interpolating polynomials as defined in Eq. (B.40). The continuous-time first-order optimality conditions of Eq. (B.37) are discretized using the variables $\mathbf{X}_0 \equiv \mathbf{X}(-1)$, $\mathbf{X}_k \equiv \mathbf{X}(\tau_k) \in \mathbb{R}^n$, and $\mathbf{X}_f \equiv \mathbf{X}(1)$ for the state; $\mathbf{U}_k \equiv \mathbf{U}(\tau_k) \in \mathbb{R}^m$ for the control; $\Lambda_0 \equiv \Lambda(-1)$, $\Lambda_k \equiv \Lambda(\tau_k) \in \mathbb{R}^n$, and $\Lambda_f \equiv \Lambda(1)$ for the costates; and $\mu_k \equiv \mu(\tau_k) \in \mathbb{R}^c$, for the Lagrange multiplier associated with the path constraints at the LG points $k = 1, \dots, N$. The other unknown variables in the problem are the initial and final times, $t_0 \in \mathbb{R}$, $t_f \in \mathbb{R}$, and the Lagrange multiplier, $\nu \in \mathbb{R}^q$. The total number of variables is then given as $(2n + m + c)N + 4n + q + 2$. These variables are used to discretize the continuous necessary conditions of Eq. (B.37) via the Gauss pseudospectral discretization. Note that the derivative of the state is approximated using Lagrange polynomials based on $N + 1$ points consisting of the N LG points and the initial time, τ_0 , while the derivative of the costate is approximated using Lagrange polynomials based on $N + 1$ points consisting of the N LG points and the final time, τ_f . The resulting algebraic equations that approximate

the continuous necessary conditions at the LG points are given as

$$\sum_{i=1}^N \mathbf{X}_i D_{ki} = \frac{t_f - t_0}{2} f_k \quad (\text{B.42})$$

$$\sum_{i=1}^N \Lambda_i D_{ki}^\dagger + \Lambda_F D_{kN+1}^\dagger = \frac{t_f - t_0}{2} \left(-\frac{\partial L_k}{\partial \mathbf{X}_k} - \Lambda_k^T \frac{\partial f_k}{\partial \mathbf{X}_k} + \mu_k^T \frac{\partial C_k}{\partial \mathbf{X}_k} \right) \quad (\text{B.43})$$

$$0 = \frac{\partial L_k}{\partial \mathbf{U}_k} + \Lambda_k^T \frac{\partial f_k}{\partial \mathbf{U}_k} - \mu_k^T \frac{\partial C_k}{\partial \mathbf{U}_k} \quad (\text{B.44})$$

$$\psi(\mathbf{X}_0, t_0, \mathbf{X}_f, t_f) = 0 \quad (\text{B.45})$$

$$\Lambda_0 = -\frac{\partial \phi}{\partial \mathbf{X}_0} + \nu^T \frac{\partial \psi}{\partial \mathbf{X}_0} \quad (\text{B.46})$$

$$\Lambda_F = \frac{\partial \phi}{\partial \mathbf{X}_f} - \nu^T \frac{\partial \psi}{\partial \mathbf{X}_f} \quad (\text{B.47})$$

$$-\frac{t_f - t_0}{2} \sum_{k=1}^N w_k \frac{\partial H_k}{\partial t_0} + \frac{1}{2} \sum_{k=1}^N w_k H_k = \frac{\partial \phi}{\partial t_0} - \nu^T \frac{\partial \psi}{\partial t_0} \quad (\text{B.48})$$

$$\frac{t_f - t_0}{2} \sum_{k=1}^N w_k \frac{\partial H_k}{\partial t_f} + \frac{1}{2} \sum_{k=1}^N w_k H_k = -\frac{\partial \phi}{\partial t_f} + \nu^T \frac{\partial \psi}{\partial t_f} \quad (\text{B.49})$$

$$\mu_{jk} = 0, \text{ when } C_{jk} < 0 \quad (\text{B.50})$$

$$\mu_{jk} \leq 0, \text{ when } C_{jk} = 0 \quad (\text{B.51})$$

for $k = 1, \dots, N$ and $j = 1, \dots, c$. The final two equations that are required (in order to link the initial and final state and costate, respectively) are

$$\mathbf{X}_f = \mathbf{X}_0 + \frac{t_f - t_0}{2} \sum_{k=1}^N w_k f_k \quad (\text{B.52})$$

$$\Lambda_F = \Lambda_0 + \frac{t_f - t_0}{2} \sum_{k=1}^N w_k \left(-\frac{\partial L_k}{\partial \mathbf{X}_k} - \Lambda_k^T \frac{\partial f_k}{\partial \mathbf{X}_k} + \mu_k^T \frac{\partial C_k}{\partial \mathbf{X}_k} \right) \quad (\text{B.53})$$

The total number of equations in the set of discrete necessary conditions of Eqs. (B.42-B.53) is $(2n + m + c)N + 4n + q + 2$ (the same number of unknown variables). Solving these nonlinear algebraic equations would be an indirect solution to the optimal control problem.

B.VI. Costate Estimate

One of the key features of the Gauss pseudospectral method is the ability to map the KKT multipliers of the NLP to the costates of the continuous-time optimal control problem. In particular, using the results of Sections B.III and B.V, a costate estimate for the continuous

Bolza problem can be obtained at the Legendre-Gauss points and the boundary points. This costate estimate is taken from²⁷ and is summarized below via the *Gauss Pseudospectral Costate Mapping Theorem*:

Theorem B.1. Gauss Pseudospectral Costate Mapping Theorem: *The Karush-Kuhn-Tucker (KKT) conditions of the NLP are exactly equivalent to the discretized form of the continuous first-order necessary conditions of the continuous Bolza problem when using the Gauss pseudospectral discretization. Furthermore, a costate estimate at the initial time, final time, and the Legendre-Gauss points can be found from the KKT multipliers, $\tilde{\Lambda}_k$, $\tilde{\mu}_k$, $\tilde{\Lambda}_F$, and $\tilde{\nu}$,*

$$\Lambda_k = \frac{\tilde{\Lambda}_k}{w_k} + \tilde{\Lambda}_F, \quad \mu_k = \frac{2}{t_f - t_0} \frac{\tilde{\mu}_k}{w_k}, \quad \nu = \tilde{\nu}, \quad \Lambda(t_0) = \tilde{\Lambda}_o, \quad \Lambda(t_f) = \tilde{\Lambda}_F \quad (\text{B.54})$$

Using the substitutions of Eq. (B.54), it can be seen that Eqs. (B.21-B.33) are exactly the same as Eqs. (B.42-B.53).

B.VII. Computation of Boundary Controls

It is seen in the GPM that the control is discretized only at the LG points and is not discretized at either the initial or the terminal point. Consequently, the solution of the NLP defined by Eqs. (B.13-B.17) does not produce values of the controls at the boundaries. The ability to obtain accurate initial and terminal controls can be important in many applications, particularly in guidance where real-time computation of the initial control is of vital interest.

At first glance, it may seem that the lack of control information at the boundaries can be overcome simply via extrapolation of the control at the LG points. However, multiple reasons exist as to why this is not the best approach. First, no particular functional form for the control is assumed in the GPM discretization. As a result, the best function to use for extrapolation is ambiguous. Second, any reasonable extrapolation of the control (e.g., linear, quadratic, cubic, or spline) may violate a path constraint which, in general, will render the extrapolated control infeasible. Third, even if the extrapolated control is feasible, it will not satisfy the required optimality conditions at the boundaries (i. e. the control will be suboptimal with respect to the NLP). Consequently, it is both practical and most rigorous to develop a systematic procedure to compute the boundary controls. The primal (state) and dual (costate) solutions of the NLP arising from the Gauss pseudospectral method are used to compute the boundary controls.²⁵

Computation of the initial control is done first since the approach for computing the terminal control is identical. First, recalling the augmented Hamiltonian, H , for the continuous-

time optimal control problem in Eq. (B.36) is

$$H(\mathbf{x}, \mathbf{u}, \lambda, \mu) \equiv L + \lambda^T f - \mu^T C \quad (\text{B.55})$$

where shorthand notation is used. Recall from the principle of Pontryagin, at every instant of time the optimal control is the control $\mathbf{u}^*(\tau) \in \mathcal{U}$ that satisfies the condition

$$H(\mathbf{x}^*, \mathbf{u}^*, \lambda^*, \mu^*) \leq H(\mathbf{x}^*, \mathbf{u}, \lambda^*, \mu^*) \quad (\text{B.56})$$

where \mathcal{U} is the feasible control set. Consequently, for a given instant of time τ where $\mathbf{x}^*(\tau)$, $\lambda^*(\tau)$, and $\mu^*(\tau)$ are known, Eq. (B.56) is a constrained optimization problem in $\mathbf{u}(\tau) \in \mathbb{R}^m$. In order to solve this constrained optimization problem at the *initial* time, it is necessary to know $\mathbf{x}^*(\tau_0)$, $\lambda^*(\tau_0)$, and $\mu^*(\tau_0)$.

Consider the information that can be obtained by solving the NLP associated with the GPM. In particular, the primal solution to the NLP produces $\mathbf{X}(\tau_0)$ while the dual solution to the NLP can be manipulated algebraically to obtain the initial costate, $\mathbf{\Lambda}(\tau_0)$. However, because the NLP does not evaluate the path constraint at the boundaries, there is no associated Lagrange multiplier $\mu^*(\tau_0)$. This apparent impediment can be overcome by applying the minimum principle in a manner somewhat different from that given in Eq. (B.56). In particular, suppose we let \mathcal{H} be the *Hamiltonian* (not the augmented Hamiltonian), where \mathcal{H} is defined as

$$\mathcal{H}(\mathbf{x}, \mathbf{u}, \lambda) \equiv L + \lambda^T f \quad (\text{B.57})$$

It is seen in Eq. (B.57) that the term involving the path constraint is not included. The path constraint is instead incorporated into the feasible control set. In particular, suppose we let \mathcal{V}_0 be

$$\mathcal{V}_0 = \mathcal{U} \cap \mathcal{C}_0 \quad (\text{B.58})$$

where \mathcal{V}_0 is the intersection of the original set of feasible controls at time τ_0 , denoted \mathcal{U} , with the set of all controls at time τ_0 that satisfy the inequality constraint of Eq. (B.17), denoted \mathcal{C}_0 . Then, using the values of $\mathbf{X}(\tau_0)$ and $\mathbf{\Lambda}(\tau_0)$, the following modified optimization problem in m variables $\mathbf{U}(\tau_0) \in \mathbb{R}^m$ can be solved to obtain the initial control, $\mathbf{U}(\tau_0)$:

$$\min_{\mathbf{U}(\tau_0) \in \mathcal{V}_0} \mathcal{H}(\mathbf{X}(\tau_0), \mathbf{U}(\tau_0), \mathbf{\Lambda}(\tau_0), \tau_0; t_0, t_f) \quad (\text{B.59})$$

It is noted that, because \mathcal{V}_0 is restricted by the inequality path constraint at τ_0 , the solution

of $\mathbf{U}(\tau_0)$ is equivalent to the solution of the following problem:

$$\begin{aligned} & \min_{\mathbf{U}(\tau_0) \in \mathcal{U}} \quad \mathcal{H}(\mathbf{X}(\tau_0), \mathbf{U}(\tau_0), \mathbf{\Lambda}(\tau_0), \tau_0; t_0, t_f) \\ & \text{subject to} \quad C(\mathbf{X}(\tau_0), \mathbf{U}(\tau_0), \tau_0; t_0, t_f) \leq 0 \end{aligned} \tag{B.60}$$

Interestingly, if the constraint is *active*, then the initial path constraint multiplier, $\mu^*(\tau_0)$, will also be determined by the minimization problem of Eq. (B.60). Finally, similar to the initial time, the control at the terminal time, $\mathbf{U}(\tau_f)$, can be obtained by solving the minimization problem of Eq. (B.60) at $\tau = \tau_f$, i. e.

$$\begin{aligned} & \min_{\mathbf{U}(\tau_f) \in \mathcal{U}} \quad \mathcal{H}(\mathbf{X}(\tau_f), \mathbf{U}(\tau_f), \mathbf{\Lambda}(\tau_f), \tau_f; t_0, t_f) \\ & \text{subject to} \quad C(\mathbf{X}(\tau_f), \mathbf{U}(\tau_f), \tau_f; t_0, t_f) \leq 0 \end{aligned} \tag{B.61}$$

The Gauss Pseudospectral Optimal Control Software (GPOCS) is a software program written in MATLAB^a for solving multiple-phase optimal control problems, which implements the algorithm as described above.

^aMATLAB is a registered trademark of The Mathworks, Inc., 3 Apple Hill Drive, Natick, MA

References

- ¹Benson, D. A., Huntington, G. T., Thorvaldsen, T. P., and Rao, A. V., "Direct Trajectory Optimization and Costate Estimation via an Orthogonal Collocation Method," *Journal of Guidance, Control, and Dynamics*, Vol. 29, No. 6, November-December 2006, pp. 1435–1440.
- ²Huntington, G. T., Benson, D. A., How, J. P., Kanizay, N., Darby, C., and Rao, A. V., "Computation of Boundary Controls using a Gauss Pseudospectral Method," *AAS/AIAA Astrodynamics Specialist Conference*, 19-23 August 2007.
- ³Rao, A. V., *User's Manual for GPOCS[©] Version 1.1: A MATLAB[®] Implementation of the Gauss Pseudospectral Method for Solving Multiple-Phase Optimal Control Problems*, Gainesville, FL 32607, August 2007.
- ⁴Nelson, D., "Qualitative and Quantitative Assessment of Optimal Trajectories by Implicit Simulation (OTIS) and Program to Optimize Simulated Trajectories (POST)," Tech. rep., Georgia Institute of Technology, 2001, AE 8900 Individual Research Project.
- ⁵Bollino, K. P., Lewis, L., Sekhavat, P., and Ross, I. M., "Pseudospectral Optimal Control: A Clear Road for Autonomous Intelligent Path Planning," *AIAA 2007 Conference and Exhibit*, 7-10 May 2007.
- ⁶Michael, I. and Fahroo, F., "A Perspective on Methods for Trajectory Optimization," *AIAA/AAS Astrodynamics and Specialist Conference and Exhibit*, 5-8 August 2002, AIAA-2002-4727.
- ⁷Fahroo, F. and Ross, I. M., "On Discrete-Time Optimality Conditions for Pseudospectral Methods," *AIAA/AAS Astrodynamics Specialist Conference and Exhibit*, 21-24 August 2006.
- ⁸Ross, I. M. and Fahroo, F., "Legendre Pseudospectral Approximations of Optimal Control Problems," *Lecture Notes in Control and Information Sciences*, Vol. 295, 2003.
- ⁹Shaffer, P. J., Ross, I. M., Oppenheimer, M. W., and Doman, D. B., "Optimal Trajectory Reconfiguration and Retargeting for a Reusable Launch Vehicle," *AIAA Guidance, Navigation, and Control Conference and Exhibit*, 15-18 August 2005.
- ¹⁰Jorris, T. R. and Cobb, R. G., "2-D Trajectory Optimization Satisfying Waypoints and No-Fly Zone Constraints," *AAS/AIAA Space Flight Mechanics Meeting*, 28 Jan - 1 Feb 2007, AAS 07-114.
- ¹¹Jorris, T. R., *Common Aero Vehicle Autonomous Reentry Trajectory Optimization Satisfying Waypoint and No-Fly Zone Constraints*, Ph.D. thesis, Air Force Institute of Technology, September 2007.
- ¹²Fornberg, B., *A Practical Guide to Pseudospectral Methods*, Cambridge University Press, 1998.
- ¹³Vinh, N. X., *Optimal Trajectories in Atmospheric Flight*, Elsevier, 1981.
- ¹⁴Bryson, Jr., A. E., *Dynamic Optimization*, Addison Wesley Longman, 1999.
- ¹⁵Vinh, N. X. and Ma, D.-M., "Optimal Multiple-Pass Aeroassisted Plane Change," *Acta Astronautica*, Vol. 21, No. 11-12, 1990, pp. 749–758.
- ¹⁶Zipfel, P. H., *Modeling and Simulation of Aerospace Vehicle Dynamics*, American Institute of Aeronautics And Astronautics, 2nd ed., 2007.
- ¹⁷*U.S. Standard Atmosphere 1976, NOAA-S/T 76-1562*, U.S. Government Printing Office, Washington D.C., 1976.
- ¹⁸Phillips, T. H., "A Common Aero Vehicle (CAV) Model, Description, and Employment Guide," Tech. rep., Schafer Corporation for AFRL and AFSPC, 27 January 2003.

¹⁹Raiszadeh, B. and Queen, E. M., “Partial Validation of Multibody Program to Optimize Simulated Trajectories II (POST II) Parachute Simulation with Interacting Forces,” Tech. rep., NASA, Langley Research Center, Hampton, Virginia, 2002, TM-2002-211634.

²⁰Bryson, Jr., A. E. and Ho, Y.-C., *Applied Optimal Control*, Taylor & Francis, 1975.

²¹DARPA, *FALCON Force Application and Launch from CONUS Task 1 Small Launch Vehicle (SLV) - Phase II*, 2004, Program Solicitation Number 04-05.

²²Rao, A. V., “Extension of a Pseudospectral Legendre Method to Non-Sequential Multiple-Phase Optimal Control Problems,” *AIAA Guidance, Navigation, and Control Conference and Exhibit*, Austin, Texas, 11-14 August 2003, AIAA 2003-5634.

²³Huntington, G. T. and Rao, A. V., “Optimal Reconfiguration of Tetrahedral Spacecraft Formations via a Gauss Pseudospectral Method,” *AAS/AIAA Astrodynamics Specialists Conference*, Lake Tahoe, CA, 7-11 August 2005, AAS 05-338.

²⁴Huntington, G. T., Benson, D. A., and Rao, A. V., “Post-Optimality Analysis and Evaluation of a Formation Flying Problem via a Gauss Pseudospectral Method,” *AAS/AIAA Astrodynamics Specialists Conference*, Lake Tahoe, CA, 7-11 August 2005.

²⁵Huntington, G. T., Benson, D. A., How, J. P., Kanizay, N., Darby, C., and Rao, A. V., “Computation of Endpoint Controls Using a Gauss Pseudospectral Method,” *Astrodynamics Specialist Conference*, Mackinac Island, Michigan, 20-23 August 2007, AAS Paper 07-381.

²⁶Huntington, G. T. and Rao, A. V., “A Comparison of Global and Local Collocation Methods for Optimal Control,” *Journal of Guidance, Control, and Dynamics*, Vol. 31, No. 2, March-April 2008, pp. 432–436.

²⁷Benson, D., *A Gauss Pseudospectral Transcription for Optimal Control*, Ph.D. thesis, Massachusetts Institute of Technology, February 2005.

²⁸Huntington, G. T., *Advancement and Analysis of a Gauss Pseudospectral Transcription for Optimal Control Problems*, Ph.D. thesis, Massachusetts Institute of Technology, June 2007.

²⁹Gong, Q., Kang, W., and Ross, I., “A Pseudospectral Method for the Optimal Control of Constrained Feedback Linearizable Systems,” *IEEE Transactions on Automatic Control*, Vol. 51, No. 7, July 2006.

³⁰Ross, I. M., Sekhavaty, P., Flemingz, A., and Gongx, Q., “Pseudospectral Feedback Control: Foundations, Examples and Experimental Results,” *AIAA Guidance, Navigation, and Control Conference and Exhibit*, Keystone, Colorado, 21-24 August 2006, AIAA 2006-6354.

³¹Elnagar, G. and Kazemi, M., “Pseudospectral Chebyshev Optimal Control of Constrained Nonlinear Dynamical Systems,” *Computational Optimization and Applications*, Vol. 11, 1998, pp. 195–217.

³²Elnagar, G., Kazemi, M., and Razzaghi, M., “The Pseudospectral Legendre Method for Discretizing Optimal Control Problems,” *IEEE Transactions on Automatic Control*, Vol. 40, No. 10, October 1995.

³³Davis, P., *Interpolation and Approximation*, Dover Publications, 1975.

³⁴Pontryagin, L., Boltyanskii, V., Gamkrelidze, R., and Mischenko, E., *The Mathematical Theory of Optimal Processes*, Interscience, New York, 1962.

³⁵Kirk, D. E., *Optimal Control Theory*, Dover Publications, 1970.